Vidal Rodriguez, B.; Mengual Chulia, T.; Martí Sendra, J. (2010). Photonic Technique for the Measurement of Frequency and Power of Multiple Microwave Signals. IEEE Transactions on Microwave Theory and Techniques. 58(11):3103-3108. https://doi.org/10.1109/TMTT.2010.2076710

Photonic Technique for the Measurement of Frequency and Power of Multiple Microwave Signals

Borja Vidal, *Member, IEEE,* Teresa Mengual, and Javier Martí, *Member, IEEE*

***Abstract*—An optical approach to simultaneously measure the frequency and power of several microwave signals is presented and demonstrated. The system is based on the processing of an interferogram generated by integrating the microwave power over the measurement band at the output of a tunable photonic microwave notch filter. Experimental results to demonstrate the principle of operation are provided showing a resolution of 15 MHz.**

***Index Terms*—Microwave measurement, microwave photonics, optical signal processing.**

I. Introduction

OPTICAL technology has a strong potential to provide alternative implementations of microwave transmission and processing systems thanks to advantages such as high time x bandwidth products, light weight, low loss and immunity to electromagnetic interference. To benefit from these advantages, different photonic implementations of microwave systems have been proposed [1].

Recently several research groups have presented schemes to measure the frequency of microwave signals using photonic architectures with the ultimate goal of developing ultra-wide bandwidth spectral analysers (especially in the millimetre and submillimeter-wave bands) without the need of multiple mixing stages as well as instantaneous frequency measurement (IFM) modules. These are particularly interesting in radioastronomy, spectrometry, radar warning receivers, electronic warfare applications as well as a new approach to microwave instrumentation.

Different innovative alternatives have been proposed to implement IFM [2]–[5], usually limited to a single frequency and some unable to determine the signal power, and spectrum analysis schemes able to resolve several simultaneous signals of different frequencies [2], [6]–[8]. This paper is devoted to the development of a new photonic-based spectrum analysis technique. Among the architectures able to resolve several frequencies, the next can be found: a scanning passband Fabry-Pérot filter [6] showing a resolution of 90 MHz and requiring a very stable scanning subsystem whose stability and repeatability limits the accuracy of the measurement; a system based on the determination of the frequency of several signals using a frequency-time mapping [7] although it was demonstrated for two RF signals spaced 20 GHz; and a spectral hole burning technique [8] which shows 1 MHz resolution but requires cryogenic cooling.

The authors are with the Nanophotonics Technology Center, Universidad Politécnica de Valencia, Valencia 46022, Spain (e-mail: bvidal@ieee.org; bvidal@ntc.upv.es; tmengual@dasphotonics.com; jmarti@ntc.upv.es).

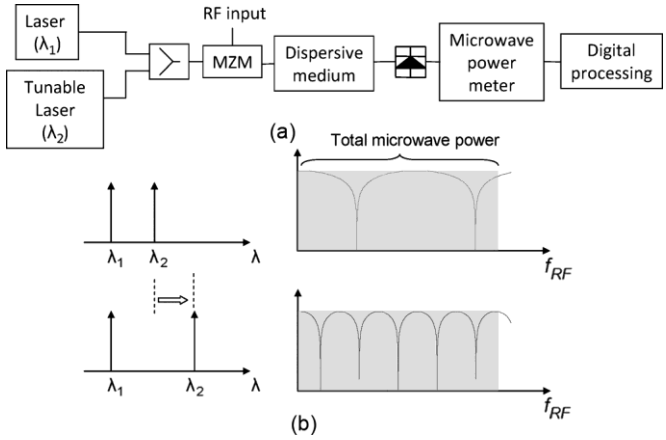

Fig. 1. Schematic of the proposed scheme (a) and principle of operation diagram (b).

This letter presents a novel photonic technique to determine the frequency and power of a set of RF signals using off-the-shelf optical communications components and digital processing. The system is based on measuring the total microwave power at the output of a tunable periodic microwave photonic notch filter. If the notch filter frequency is swept, the microwave power changes depending on the frequency of the input signals and the filter parameters. These measurements generate an interferogram. The spectral components of the RF input can be measured by processing the interferogram. Thus, RF power and frequency of a multiplicity of incoming signals can be measured over a wide bandwidth. This technique can be related to Fourier Transform Spectrometry and similar schemes for optical spectrum analysis [10], [11].

II. System Description

Fig. 1 shows the block diagram of the proposed photonic approach for microwave power and frequency measurement.

It consists of a CW fixed laser and a CW tunable laser of the same output power. Both optical carriers are amplitude modulated by an external modulator (e.g., Mach–Zehnder modulator, MZM) fed with the microwave signals to be measured. After amplitude modulation the signals are launched to a dispersive

medium (e.g., a fiber coil) and photodetected. Dispersion introduces a time delay ($\Delta\tau$) between the optical carriers given by

$$\Delta\tau = L \cdot \int_{\lambda_1}^{\lambda_2} D(\lambda)d\lambda = \frac{L \cdot S_0}{8}\left(\lambda_2^2 - \lambda_1^2\right)\left[1 - \frac{\lambda_0^4}{\lambda_1^2\lambda_2^2}\right] \quad (1)$$

where S_0 is the fiber dispersion slope parameter ($\mathrm{ps/nm^2 \bullet km}$), L is the length of the dispersive medium (km) and λ_1 and λ_2 are the wavelengths of the optical carriers (nm). Since both optical carriers are modulated with the same microwave signal, there are two copies of the signal at the output of the photodiode with a time delay between them given by (1), i.e., a periodic microwave notch filter is generated [8]. After the photodiode, a microwave power meter measures the total power of the filtered signal. If the wavelength spacing ($\Delta\lambda = \lambda_2 - \lambda_1$) between optical carriers is changed (using a tunable laser), the time delay between optical carriers is modified and the free-spectral range (FSR) of the notch filter changes. That results in a different combination of filtered frequencies and a different value of the total microwave power at the output of the photodiode. If this process is repeated, an interferogram is composed with one point for each wavelength spacing between optical carriers. Finally, the RF spectrum can be obtained performing the Fast Fourier Transform (FFT) over the interferogram data.

Spectral resolution is given by the maximum time delay between optical carriers, i.e., its minimum FSR. The higher the time delay, the smaller the frequency spacing between FFT points. On the other side, the maximum RF bandwidth is limited by the bandwidth of the external modulator, photodiode and microwave power meter. There are commercial devices of all of them with bandwidths exceeding 40 GHz. Additionally, FFT processing limits the maximum RF frequency. Thus, the system frequency range is the minimum between the bandwidth given by the system spectral resolution and the number of FFT points and the bandwidth of electrooptic and optoelectronic conversions.

III. Theory

Let it be a signal, $s(t)$, to be measured and whose Fourier Transform (FT) is given by $S(f)$. The output of the microwave power meter (Fig. 1) is the product of the unknown signal and the notch filter transfer function

$$RF\ power = \frac{1}{2\pi}\int_0^{f_{\max}} \left|S'(f)\cdot H(f)\right|^2 df \quad (2)$$

where f_{max} is the maximum RF frequency, $S'(f)$ is the Fourier Transform of the signal under test at the output of the photodiode and $H(f)$ is the notch filter transfer function generated by the fiber coil which is given by

$$H(f) = 1 + \cos(2\pi f \Delta\tau) \quad (3)$$

where $\Delta\tau$ is the time delay generated by the fiber coil dispersion as given by (1). If the total microwave power is measured for a set of values of $\Delta\tau$, an interferogram is composed. The RF spectrum can be obtained from the Fourier Transform of this set of measurements

$$\text{RF Spectrum} = FT\left\{\frac{1}{2\pi}\int_0^{f_{\max}} \left|S'(f)\ \ (1+\cos(2\pi f\Delta\tau))\right|^2 df\right\} \quad (4)$$

Due to changes in chromatic dispersion with wavelength (1), $\Delta\tau$ is not constant over the $\lambda_1\lambda_2$ range and therefore the interferogram points are unevenly spaced. Two approaches to obtain the Fourier Transform of an uneven set of data have been explored: data interpolation to obtain a new evenly spaced interferogram and the Lomb-Scargle periodogram [12]. Due to its simplicity the first option was preferred.

The signal under test at the output of the photodiode ($s'(t)$) can be calculated from the general expressions of radio-over-fiber links based on external modulation [13]. Assuming that the signal under test is a tone for the sake of clarity, the amplitude modulated optical field at the output of a dual drive MZM (DD-MZM) can be expressed as

$$\vec{E} = \frac{\sqrt{L_{\mathrm{MZM}}}E_o}{2\cdot}\left\{e^{-i\left(\omega_c t - kz + \frac{\pi V_{\mathrm{DC1}}}{V_\pi(\mathrm{DC})} + \frac{\pi V_{RF}}{V_\pi(f_{RF})}\cos(\omega_{RF}t+\phi_1)\right)}\right.$$
$$\left. + e^{-i\left(\omega_c t - kz + \frac{\pi V_{\mathrm{DC2}}}{V_\pi(\mathrm{DC})} + \frac{\pi V_{RF}}{V_\pi(f_{RF})}\cos(\omega_{RF}t+\phi_2)\right)}\right\} \quad (5)$$

where ω_c and ω_{RF} are the angular frequency of the optical carrier and the RF signal, respectively, $\mathrm{V_{RF}}$ is the amplitude of modulating signal, V_π is the MZM switching voltage and $\mathrm{L_{MZM}}$ is the MZM loss. In order to generate an optical single-sideband modulation, the DD-MZM has to be biased at the linear point $|\mathrm{V_{DC1}} - \mathrm{V_{DC2}}| = \mathrm{V}_\pi/2$, with a phase shift between MZM drivers $|\Phi_{\mathrm{RF1}} - \Phi_{\mathrm{RF2}}| = \pi/2$.

Equation (5) can be expanded in terms of Bessel functions of the first kind and assuming a small signal scenario (i.e., low modulation index, $\mathrm{m} = \pi\mathrm{V_{RF}}/\mathrm{V}_\pi(f_{RF})$ only the terms depending on Bessel functions of zero and first order can be considered, and higher order functions can be neglected. As a result, (5) can be simplified as

$$\vec{E} = \frac{\sqrt{L_{MZ}}E_o}{2\cdot}\left\{J_0(m)\left[e^{-i(\omega_c t - kz)} + e^{-i\left(\omega_c t - kz + \frac{\pi}{2}\right)}\right]\right.$$
$$\left. + J_1(m)e^{-i\left((\omega_c+\omega_{RF})t - kz + \frac{\pi}{2}\right)}\right\} \quad (6)$$

If the losses caused by fiber coil are taken into account, the electrical field at the output of the proposed system can be expressed as

$$\vec{E}_{\mathrm{out}} = \sqrt{L_{Coil}}\vec{E}. \quad (7)$$

Thus, the signal at the photodiode is (8), shown at the bottom of the following page, where $\Re$ and G are the responsivity and gain of the photodiode, respectively.

Therefore, taking into account (8) the RF spectrum of the signal under test, (4), can be expressed as

$$\text{RF Spectrum} \propto \Re \cdot \mathrm{G} \cdot \mathrm{L_{MZM}} \mathrm{L_{Coil}} \mathrm{E_o^2} [\mathrm{J_0(m)} \mathrm{J_1}(m) \delta(\omega - \omega_{\mathrm{RF}})] \tag{9}$$

Assuming low modulation indexes

$$\begin{aligned} \mathrm{J_0(m)} &\cong 1 \\ \mathrm{J_1(m)} &\cong \frac{m}{2}. \end{aligned} \tag{10}$$

Equation (9) can be rewritten as

$$RF\ Spectrum \propto \Re \mathrm{G} \mathrm{L_{MZM}} \mathrm{L_{Coil}} \mathrm{E_o^2} \frac{\pi \mathrm{V}_{RF}}{2V_\pi(f_{RF})} \delta(\omega - \omega_{\mathrm{RF}}). \tag{11}$$

From (11), it can be seen, that the technique allows the measurement of both frequency and power and that it can be extended to several simultaneous RF signals. Additionally, although the technique does not provide instantaneous measurements, each point of the interferogram is obtained from the total microwave power. Thus, the capability to detect incoming signals is improved in scenarios where low probability of interception techniques are used. The system will also introduce latency due to the propagation time delay experienced by the signal when crossing the fiber coil. Thus, the total response time of the technique will be given by the time required by the tunable laser swept plus the propagation time delay needed to cross the fiber coil.

If signals with high RF power are present at the system input, the small signal approximation of (5) cannot be done and additional nonlinear terms will degrade the measurement performance as in radio-over-fiber links. To overcome this issue in radio over fiber systems, electrooptical linearization schemes have been proposed (e.g., [14]), although in this case there are two optical carriers and the wavelength of one of the carriers varies, so the linearization of the system can be more complex than in conventional radio over links. The system performance in terms of sensitivity and dynamic range can be derived from expressions for conventional analog radio over fiber links [15].

IV. System Evaluation

To assess the robustness of the technique and relate performance with design parameters, several simulations have been carried out assuming a coil of 25 km of standard single mode fiber as dispersive element ($\mathrm{S_0} = 90.85\ \mathrm{fs/(nm^2\ km)}$) and a RF tone at 2.5 GHz as signal under test.

Figs. 2 and 3 show how errors in the wavelength spacing between optical carriers translate to the power and frequency measurements for different maximum wavelength sweep ranges. Steps in Fig. 3 are caused by limited RF frequency resolution. For a wavelength error lower than 1 nm the frequency error would be better than 2 MHz.

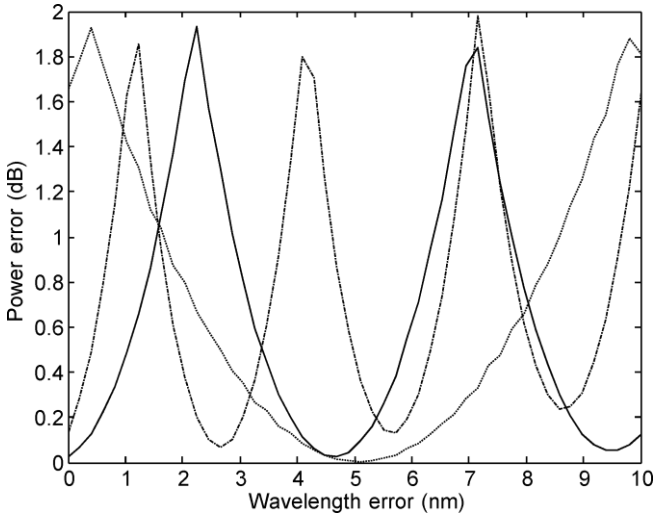

Fig. 2. Effect of errors in the microwave power measurement due to errors in the wavelength spacing between optical carriers for different wavelength swept ranges: 30 nm (dotted line), 60 nm (solid line), and 100 nm (dash dotted line).

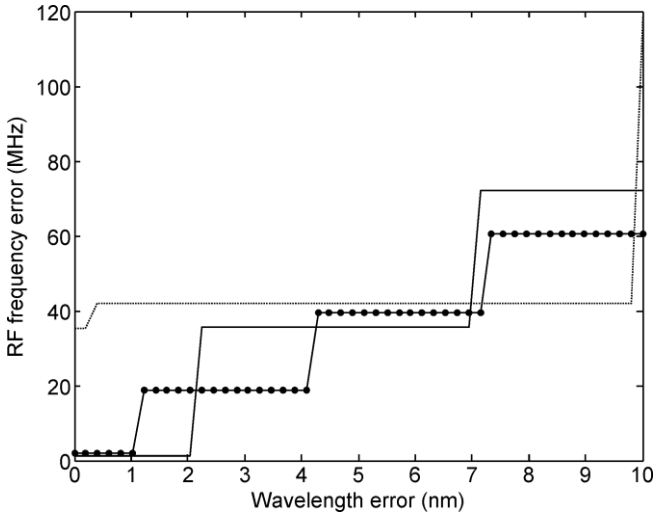

Fig. 3. Effect of errors in the microwave frequency measurement due to errors in the wavelength spacing between optical carriers for different wavelength swept ranges: 30 nm (dotted line), 60 nm (solid line), and 100 nm (dash dotted line).

Figs. 4 and 5 depict the effect of power unbalance between optical carriers in the RF power and frequency measurements. A linear dependence between optical power errors and RF power errors can be appreciated. RF power errors for conventional cooled optical sources are well below 2 dB. On the other side, RF frequency measurements are independent of the

$$s'(t) = \sqrt{\Re \mathrm{G} \mathrm{L_{MZM}} \mathrm{L_{Coil}} \frac{\mathrm{E}}{2} \left\{ \mathrm{J_0^2}(m) + 2\mathrm{J_1^2}(m) + 2\sqrt{2}\mathrm{J_0}(m)\mathrm{J_1}(m)(\cos\left[\omega_{\mathrm{RF}} t + \frac{\pi}{4}\right] \right\}} \tag{8}$$

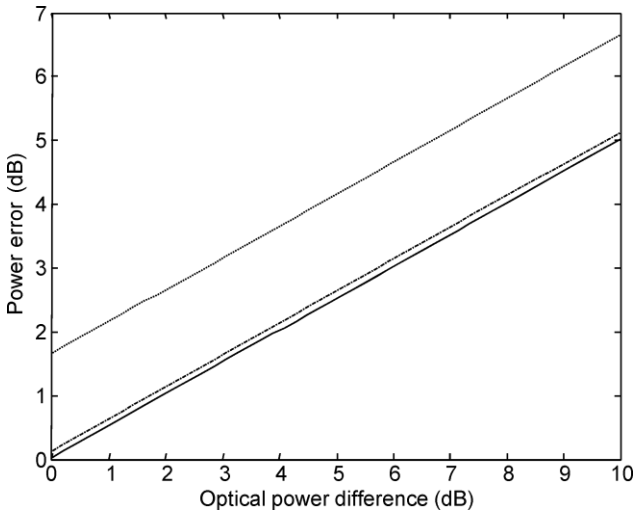

Fig. 4. Effect of errors in the microwave power measurement due to optical power unbalance between both optical carriers for different wavelength swept ranges: 30 nm (dotted line), 60 nm (solid line), and 100 nm (dash dotted line).

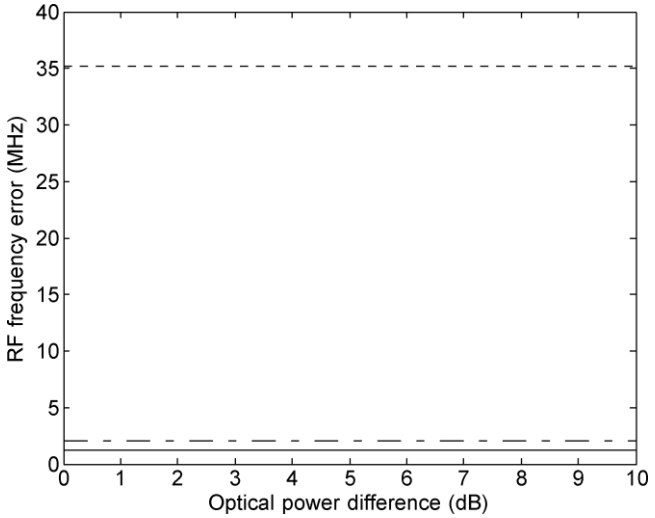

Fig. 5. Effect of errors in the microwave frequency measurement due to optical power unbalance between both optical carriers for different wavelength swept ranges: 30 nm (dotted line), 60 nm (solid line), and 100 nm (dash dotted line).

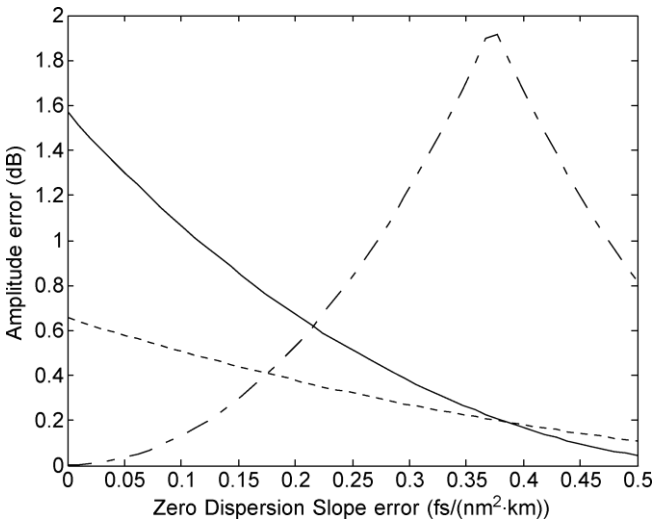

Fig. 6. Effect of errors in the microwave power measurement due to errors in the determination of the fiber dispersion parameter for different wavelength swept ranges: 30 nm (dotted line), 60 nm (solid line), and 100 nm (dash dotted line).

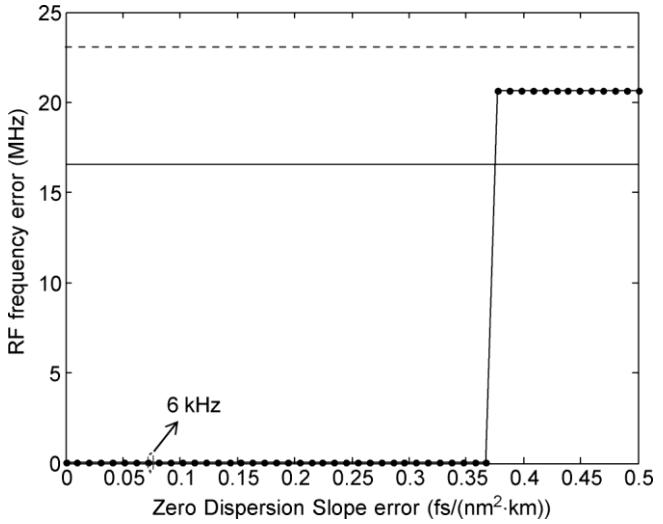

Fig. 7. Effect of errors in the microwave frequency measurement due to errors in the determination of the fiber dispersion parameter for different wavelength swept ranges: 30 nm (dotted line), 60 nm (solid line), and 100 nm (dash dotted line).

optical power balance between optical carriers depending on the wavelength sweep range (the larger the range the better the frequency resolution).

Finally, Figs. 6 and 7 show the impact of chromatic dispersion characterization on the measurements. Fiber dispersion characterization equipment usually provides measurements with uncertainty better than 0.04 $\mathrm{fs}/(\mathrm{nm}^2\ \mathrm{km})$ and temperature dependence, which depends on the fiber type, can be around $4.5 \cdot 10^{-3}\ (\mathrm{fs}/(\mathrm{nm}^2 \cdot \mathrm{km}))^{\circ}\mathrm{C}$ [16]. From these figures it can be seen that the effect of errors in dispersion characterization is small for large wavelength sweeps.

V. Experimental Setup and Results

Proof-of-concept experiments using the setup of Fig. 8 were performed to verify the feasibility of the technique. Two optical sources, each having an output power of 6 dBm, were used: a fixed laser at 1548 nm and a tunable laser. A dual drive Mach–Zehnder Modulator (DD-MZM), DC biased to operate at quadrature, was employed as an external modulator. A DD-MZM was chosen to modulate the optical carriers with a single sideband modulation (SSB) and thus avoid dispersion-based fading. The dispersive element was implemented using a coil of standard single mode fiber (SSMF) of 50.04 km and with a dispersion parameter of 16.85 ps/(nm km), a zero dispersion wavelength (λ_0) of 1317.04 nm and a dispersion slope of 90.85 $\mathrm{fs}/(\mathrm{nm}^2\mathrm{km})$. The use of dispersion compensating fiber or other high dispersive fiber would improve the compactness and/or resolution of the system.

A tone at 3 GHz was used as test signal. Fig. 9 shows the interferogram obtained when a measurement of 501 points was carried out using a tunable laser sweep between 1549 and 1568 nm (i.e., $\Delta\lambda = 1$–20 nm). From these data, the RF spectrum

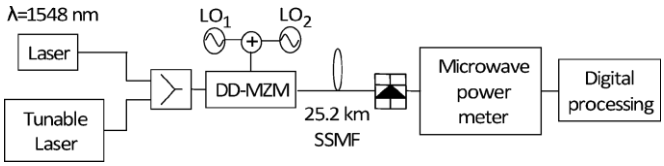

Fig. 8. Experimental setup for proof of concept.

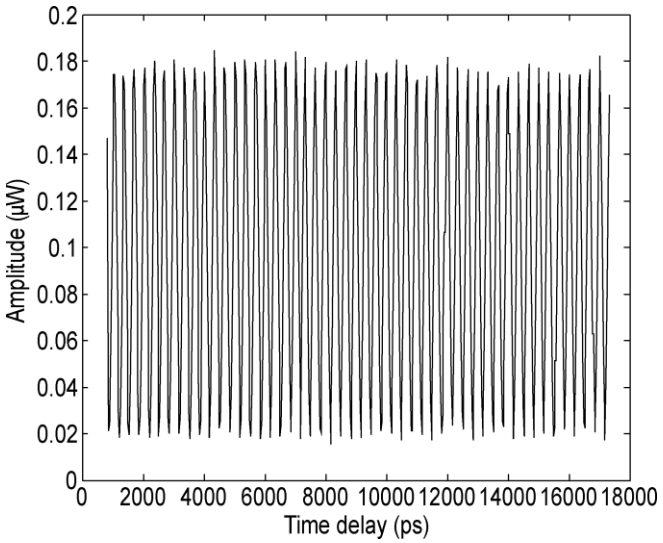

Fig. 9. Measured interferogram for one tone at f_{LO} == 3 GHz and 8.6 dBm.

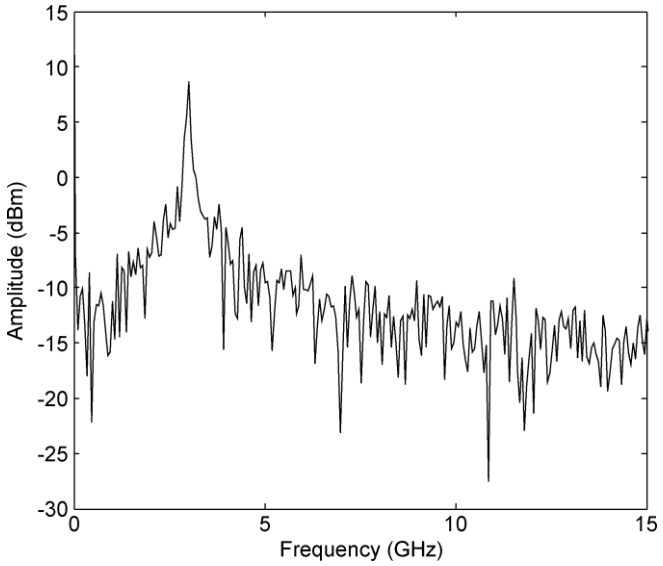

Fig. 10. RF spectrum derived from the interferogram shown in Fig. 9.

can be inferred using the processing described in Section II as shown in Fig. 10. As it can be seen, one tone with a peak at 3.015 GHz is clearly shown in the measurement. The power of the tone can also be measured to be 8.64 dBm. These measurements were carried out for different input powers as shown in Table I where the results obtained with the technique are compared with a spectrum analyzer. Both frequency and power measurements show a good agreement between the measured values and the expected ones.

TABLE I
RF FREQUENCY AND POWER MEASURED OF THE SIGNAL UNDER TEST (SYSTEM INPUT)

Photonic technique		Spectrum analyzer	
Frequency (GHz)	**Power (dBm)**	**Frequency (GHz)**	**Power (dBm)**
3.015	8.64	3.000	8.51
3.015	6.31	3.000	6.49
3.015	4.55	3.000	4.50

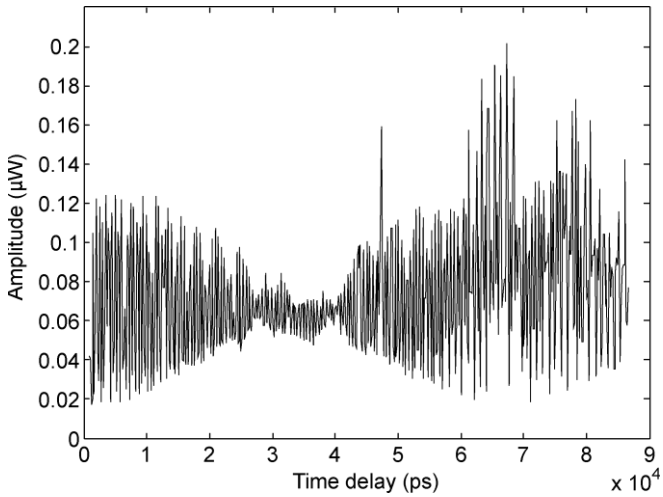

Fig. 11. Measured interferogram for a tone at f_{LO1} == 2 GHz and f_{LO2} == 2 015 GHz.

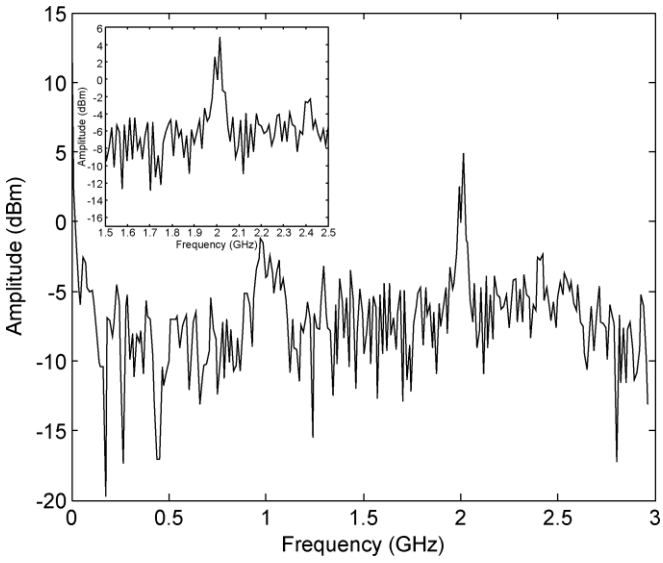

Fig. 12. RF spectrum measured for two RF tones at f_{LO1} == 2 GHz and f_{LO2} == 2 015 GHz. The inset shows a zoom around 2 GHz.

Tests were done using two RF tones spaced 15 MHz ($f_{LO1} = 2$ GHz and $f_{LO2} = 2.015$ GHz) to assess the frequency resolution of the system. A sweep of the tunable laser from 1549 to 1639 nm (i.e., $\Delta\lambda =$ 1–90 nm) was employed. Fig. 11 depicts

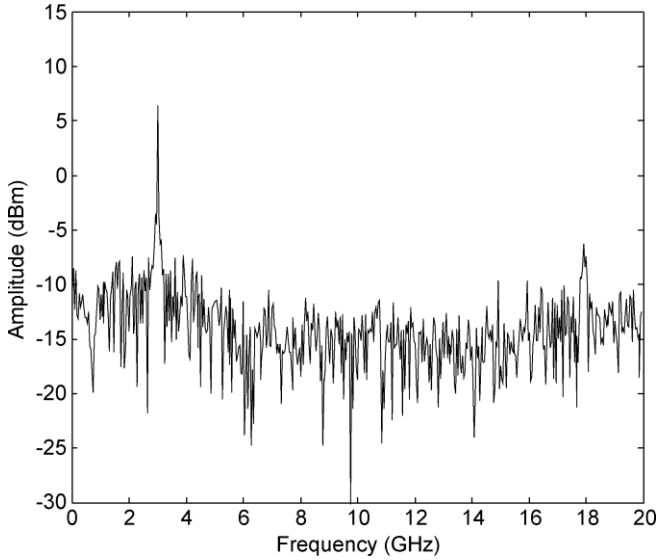

Fig. 13. RF spectrum measured for two RF tones at f_{LO1} = GHz and f_{LO2} = 18 GHz.

the interferogram and Fig. 12 the RF spectrum derived from the former. Two tones can be resolved, being their measured frequencies 1.992 and 2.015 GHz, respectively. It agrees well with the expected value.

Finally, to show the capability of the technique to operate in a broad bandwidth, a measurement has been carried out between DC and 19 GHz using two tones as test signals one LO at $f_{LO1} = 3$ GHz and other one at $f_{LO2} = 18$ GHz. As it can be seen in Fig. 13 two tones at these frequencies can be resolved. The low power detected at 18 GHz is mainly due to the limited bandwidth of the electrooptical and optoelectronic components used in the setup.

VI. Conclusion

A novel photonic-based alternative approach to RF spectrum measurement has been proposed using a simple setup. The technique shows broad bandwidth, simplicity, capability to measure several signals simultaneously, robustness as well as good resolution. Experiments have demonstrated the principle of operation with a resolution of 15 MHz. However, further work is needed to improve resolution, dynamic range and operational bandwidth at frequency bands beyond 50 GHz where conventional pure microwave techniques present limited performance and photonics could provide a competitive alternative.

Acknowledgment

This work was supported in part by the Spanish Ministerio de Ciencia e Innovacion under project TEC2009-08078.

References

[1] J. Capmany and D. Novak, "Microwave photonics combines two worlds," *Nature Photonics*, vol. 1, p. 319, 2007.

[2] L. V. T. Nguyen and D. B. Hunter, "A photonic technique for microwave frequency measurement," *IEEE Photon. Technol. Lett.*, vol. 18, no. 10, pp. 1188–1190, May 2006.

[3] X. Zou and J. Yao, "An optical approach to microwave frequency measurement with adjustable measurement range and resolution," *IEEE Photon. Technol. Lett.*, vol. 20, no. 23, pp. 1989–1991, Dec. 2008.

[4] H. Emami, N. Sarkhost, L. A. Bui, and A. Mitchell, "Amplitude independent RF instantaneous frequency measurement system using photonic Hilbert transform," *Opt. Exp.*, vol. 16, no. 18, pp. 13707–13712, Sep. 2008.

[5] J. Li, S. Fu, K. Xu, J. Q. Zhou, P. Shum, J. Wu, and J. Lin, "Photonic-assisted microwave frequency measurement with higher resolution and tunable range," *Opt. Lett.*, vol. 34, no. 6, pp. 743–745, Mar. 2009.

[6] S. T. Winnall and A. C. Lindsay, "A Fabry–Perot scaning receiver for microwave signal processing," *IEEE Trans. Microw. Theory Tech.*, vol. 47, pp. 1385–1390, Jul. 1999.

[7] L. V. T. Nguyen, "Microwave photonic technique for frequency measurement of simultaneous signals," *IEEE Photon. Technol. Lett.*, vol. 21, no. 10, pp. 642–644, May 2009.

[8] L. Ménager, I. Lorgeré, J. L. Le Gouët, D. Dolfi, and J. P. Huignard, "Demonstration of a radio-frequency spectrum analyzer based on spectral hole burning," *Opt. Lett.*, vol. 26, no. 16, pp. 1245–1246, Aug. 2001.

[9] D. Norton, S. Johns, C. Keefer, and R. Soref, "Tunable microwave filter using high dispersion fiber time delays," *IEEE Photon. Technol. Lett.*, vol. 6, no. 7, pp. 831–832, Jul. 1994.

[10] B. C. Smith, *Fundamentals of Fourier Transform Infrared Spectroscopy*. Boca Raton, FL: CRC Press, 1996.

[11] D. M. Baney, B. Szafraniec, and A. Motamedi, "Coherent optical spectrum analyzer," *IEEE Photon. Technol. Lett.*, vol. 14, no. 3, pp. 355–357, Mar. 2002.

[12] W. H. Press, S. A. Teukolsky, W. T. Vetterling, and B. P. Flannery, *Numerical Recipes*, 3rd ed. Cambridge, U,K.: Cambridge Univ. Press, 2007.

[13] J. L. Corral, J. Marti, and J. M. Fuster, "General expressions for IM/DD dispersive analog optical links with external modulation or optical up-conversion in a Mach–Zehnder electrooptical modulator," *IEEE Trans. Microw. Theory Techn.*, vol. 49, no. 10, pp. 1968–1976, Oct. 2001.

[14] E. I. Ackerman, "Broad-band linearization of a Mach–Zehnder electrooptic modulator," *IEEE Trans. Microw. Theory Techn.*, vol. 47, no. 12, Dec. 1999.

[15] C. H. Cox, *Analog Optical Links*. Cambridge, U,K.: Cambridge Univ. Press, 2004.

[16] M. J. Hamp, J. Wright, L. Hubbard, and B. Brimacombe, "Investigation into the temperature dependence of chromatic dispersion in optical fiber," *IEEE Photon. Technol. Lett.*, vol. 14, no. 11, pp. 1524–1546, Nov. 2002.